Applied Surface Science 322 (2014) 41–46

Contents lists available at ScienceDirect

Applied Surface Science

journal homepage: www.elsevier.com/locate/apsusc

In vitro biocompatibility response of Ti–Zr–Si thin film metallic glasses

J.L. Ke, C.H. Huang, Y.H. Chen, W.Y. Tsai, T.Y. Wei, J.C. Huang*

Department of Materials and Optoelectronic Science, National Sun Yat-Sen University Kaohsiung, 804, Taiwan, ROC

ARTICLE INFO

Article history:
Received 14 August 2014
Received in revised form
10 September 2014
Accepted 13 September 2014
Available online 25 October 2014

Keywords:
Ti
Metallic glass
Biomaterials
Electrochemical
Corrosion

ABSTRACT

In this study, the bio-electrochemical response of the Ti–Zr–Si thin film metallic glasses (TFMGs) in simulated body fluid with different contents of titanium is measured via potentiostat. According to the results of bio-corrosion potential and current, as well as the polarization resistance, it is concluded that the $Ti_{66}Zr_{25}Si_9$ TFMGs possess the highest bio-electrochemical resistance. With increasing content of titanium, the corrosion resistance becomes progressively higher. The passive current results reveal that amorphous alloys can form a more protective and denser passive film on the metallic glass surface than the crystalline materials. In addition, the mechanical performance of the Ti–Zr–Si TFMGs is better than the crystalline counterparts. As a result, the Ti-based TFMGs are considered to be potential materials for bio-coating applications.

1. Introduction

There have been numerous crystalline metallic alloys developed so far, showing acceptable in vitro and in vivo biocompatibility response, along with chemical and mechanical stability. These include Ti-based, stainless-steel-based, Ta-based, Co-based, etc. [1–6]. While the matrix elements such as Ti and Ta are highly bio-friendly for long-termed implant in human body, the incorporated secondary or trace elements, such as Ni, Cu, Al, or even Be, are frequently related to toxic, allergic or carcinogenic unwanted symptoms. Also, most of the crystalline bio-friendly alloys tend to possess an elastic modulus much higher than the human bone, potentially inducing stress shielding problems. If the crystalline alloys are fabricated into porous foams, this can be solved, but the resulting tensile or compressive strength of such foams tends to be lower than expectation. Thus, it is always of need to develop new metallic materials with lower modulus but higher strength.

Metallic glasses, or amorphous metals/alloys, are another category of metallic materials, characteristic of lower elastic modulus (due to the random atomic packing and the presence of free volume) but much higher strength (due to the absence of lattice defects such as dislocations or stacking faults). These characteristics, which are in opposite direction with respect to the crystalline counterparts, can be attractive for the bio-implant purpose.

For bio-friendly concerns, there have been a number of bulk metallic glasses (BMG) [7–14], thin film metallic glasses (TFMGs) [15,16], or porous metallic glass foams (PMGFs) [17–19] developed and studied. Ti-based MGs have also been researched. These include Ti–Cu–Ni [7], Ti–Cu–Ni–Co [8], Ti–Cu–Ni–Zr [9], Ti–Cu–Ni–Zr–Sn [10], Ti–Cu–Ni–Sn–B–Si [11], Ti–Cu–Ni–Zr–Be [12], etc. Some of the unfavorable elements are sometimes still added in such metallic glasses to improve the glass forming ability (GFA), including Ni, Cu, Al, and Be. For common Ti based, stainless steel based, or Co based crystalline alloys, Ni, Cu and Be are not typically added. But for amorphous metallic glasses, Cu, Ni or Be are almost universally added to improve their glass forming ability, taking advantages of the smaller atomic sizes of Cu or Be to randomize the atomic packing. Toxic-element-free metallic glasses have also been proposed, mostly in the form of rapid-cast rods or melt-spun ribbons. For example, from 2007, Inoue's group developed the Ni-free Ti-based metallic glasses such as the Ti–Zr–Cu–Pd and Ti–Zr–Cu–Pd–Sn BMGs [13,14] which exhibited good corrosion resistance, high strength and good glass-forming ability. In the same year, Zhu et al. [20] and Qin et al. [13] investigated Ti-based BMGs without any toxic elements. In 2013, Mariana et al. [21] developed the two Ti-based amorphous bulk alloys which are Ti–Zr–Si and Ti–Zr–Nb–Si. With the addition of Nb, Ti–Zr–Nb–Si exhibits the better bio-corrosion resistance than Ti–Zr–Si.

* Corresponding author. Tel.: +886 7 525 4070; fax: +886 7 525 4099.
E-mail address: jacobc@mail.nsysu.edu.tw (J.C. Huang).

http://dx.doi.org/10.1016/j.apsusc.2014.09.204
0169-4332/

In contrast to the Ti-based BMGs, there have been very limited reports on the TFMGs with no unwanted element for bio-implant. In this study, we report, for the first time, a series of Ti–Zr–Si based TFMGs. The mutual heat of mixing for Ti–Zr, Zr–Si and Ti–Si is either near zero or negative (being 0, −84 and −66 kJ/mol, respectively), and the atomic radius of Ti, Zr and Si is ~1.48, 1.60 and 1.10 Å, making this Ti–Zr–Si ternary system possible to form amorphous structure, especially under the more 'violent' sputtering deposition process. Their promising biocompatibility and mechanical properties are presented and discussed in this paper.

2. Experimental procedures

For TFMGs, the $Zr_{43}Ti_{43}Si_{14}$ (in at%) alloy target and pure Ti target, 50.8 mm in diameter and purchased from Well Being Enterprise Company, Taiwan, were used for the magnetic sputtering deposition. The purity levels of the alloy and Ti sputtering targets are 99.7% and 99.95%, respectively. The polished pure Ti sheet, with the area size of $10 \times 10\,mm^2$, was used as substrate. Both targets are placed on the DC cathodes. A rotary pump was used to achieve mediate vacuum, and a cryo-pump was used to achieve a base pressure below 5×10^{-7} Torr. After achieving the base pressure, Ar was introduced into the chamber, and targets were pre-sputtered by inserting a movable shutter for 5 min, maintaining a working pressure of 3×10^{-3} Torr. By adjusting the powers of the two DC cathodes, three Ti-based TFMGs can be prepared. Pure Ti films are also prepared for comparison. All films were deposited to a thickness about 600 nm, as measured by the 3D alpha-step profilometer.

The nature of the as-deposited Ti–Zr–Si and pure Ti thin films was examined by X-ray diffraction (XRD), with a monochromatic Cu-K_α radiation ($\lambda = 1.5406$ Å), worked at 40 kV and 30 mA, and equipped with 0.02 mm graphite monochrometer, was employed. The scanning range of diffraction angle is from 20° to 60° with 0.1 steps for 4 s. The JEOL JSM-6330 scanning electron microscopy (SEM), with energy dispersive spectrometry (EDS), is applied to reveal the microstructure, morphology and chemical composition of the resulting films. The average roughness (Ra) was measured by atomic force microscopy (AFM). The JEOL JPS-9010MX X-ray photoemission spectroscopy (XPS), using mono Mg-K_α radiation at vacuum pressure of $\sim 10^{-9}$ Torr, 10 kV, and 5 mA, is adopted to analyze the surface composition of the thin film after the immersion test under simulation body-fluid (SBF) for seven days. The binding energy was calibrated using the C-ls hydrocarbon peak at 284.2 eV. For the basic mechanical properties, the thin films were investigated by MTS nanoindenter XP device under the continuous stiffness measurement (CSM) mode with strain rate of 0.01 s^{-1}. To prevent from the substrate effect, the indented depth has to be less than 10% of the film thickness, or about 60 nm.

The electrochemical behavior and bio-corrosion properties of the Ti–Zr–Si TFMGs in 40 mL simulated body fluid (SBF or Hank's solution, pH: 6.5) at 37 °C were tested by electrochemical polarization measurements which were conducted by a CHI 614D electrochemical work station in a three electrodes cell. The counter and reference electrode are platinum wire and Ag/AgCl, and specimens were used to be a working electrode with an immersion area of about 0.36 cm^2. The state of electrochemical surrounding with specimens has to be steady in SBF until the open-circuit potential (OCP) changed by no more than 2 mV/10 min before the potentiodynamic polarization measurements and maintained up to 12,500 s. The anodic polarization scan is measured from −1 V to 2 V with a scan rate 0.3 mV/s. The corrosion current density (I_{corr}), corrosion potential (E_{corr}) and corrosion rate can be determined by the Tafel extrapolation method from the anodic polarization plots. The electrochemical impedance spectroscopy technique (EIS) is preformed to investigate the property of passive film formed on the surface of the Ti–Zr–Si films. The impedance spectra were acquired in the frequency range of 10^{-2}–10^5 Hz, and the potential amplitude was set to 0.01 V in open circuit potential. To ensure that the electrochemical testing system is indeed under the steady state, it is necessary to let the samples be immersed in the SBF for 12,500 s (the open circuit potential changed by no more than 2 mV/10 min) before the EIS test.

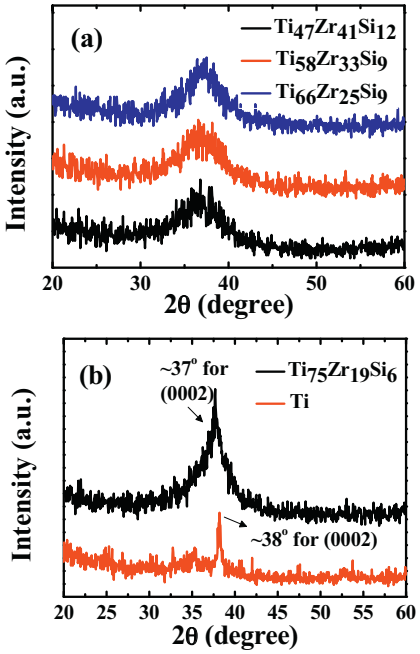

Fig. 1. The XRD patterns of the three TiZrSi as-deposited thin films.

3. Results and discussion

3.1. Basic film property characterization

Five sputtered thin films were successfully prepared by careful adjustment of the cathode powers. The resulting chemical composition of each film was measured by SEM/EDS for multiple times, and was determined to be $Ti_{47}Zr_{41}Si_{12}$, $Ti_{58}Zr_{33}Si_9$, $Ti_{66}Zr_{25}Si_9$, $Ti_{75}Zr_{19}Si_6$ and pure Ti with increasing Ti target power. The composition is seen to be quite uniform over the film area; composition scattering was all within ±1 at% Then thin film specimens were investigated by XRD, as demonstrated in Fig. 1. Three of them show diffuse hump characteristic of the amorphous structure nature in Fig. 1(a). This is not surprising since sputtering usually yields a wider composition window to result in amorphous metallic glass films. The fully amorphous nature of the three films, $Ti_{47}Zr_{41}Si_{12}$, $Ti_{58}Zr_{33}Si_9$, $Ti_{66}Zr_{25}Si_9$, has also been confirmed by detailed transmission electron microscopy (not shown). The Ti–Zr based TFMGs are seen to be much easier to form fully amorphous phase by sputtering, as compared with suction rapid quenching.

When the Ti content reached 75 at% the diffuse hump is superimposed with a sharper peak at 2θ ~37° which can be indexed by the (0 0 0 2) peak of the hexagonal close-packed (HCP) α phase in Fig. 1(b). Materials of the amorphous metallic glassy matrix with embedded nanocrystalline particles are generally termed as thin film metallic glass composites (TFMGCs). The composition of about $Ti_{80}Zr_{20}$ (in at%) as measured by EDS. Ti and Zr are mutually completely soluble, forming a isomorphous phase diagram. With the incorporation of a larger sized Zr atoms (atomic radius of Zr~0.160 nm) into the Ti HCP lattice (atomic radius of Ti~0.148 nm), the c-constant become larger to a value of 0.477 nm

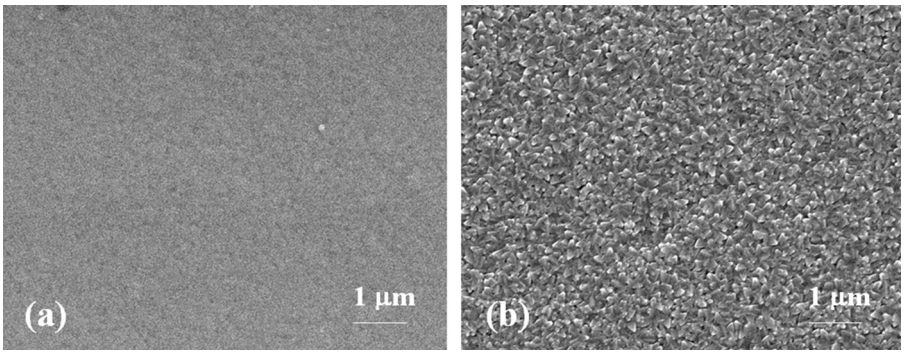

Fig. 2. SEM/SEI images of the sputtered thin films: (a) the fully amorphous $Ti_{66}Zr_{25}Si_9$ film, and (b) the crystalline pure Ti film.

from the c-constant of 0.468 nm for pure Ti. Thus the (0 0 0 2) XRD 2θ peak for the $Ti_{75}Zr_{19}Si_6$ film is slightly shifted to a smaller 2θ position of ~37°. For the pure Ti film, the (0 0 0 2) 2θ peak is located at the ~38°, as expected. Note that the HCP Ti lattice for deposited thin films tends to possess very strong basal plane texture, thus only one (0 0 0 2) peak can be seen in Fig. 1(b).

The size of the nanocrystalline Ti or Ti(Zr) α phase was estimated by the simple Scherrer equation [22], without the consideration of residual stress term. Multiple measurements have been conducted on the dominant Ti or Ti(Zr) (0 0 0 2) peak. The results reveal that the α-phase particle size is only around 3 ± 1 nm for the as-deposited $Ti_{75}Zr_{19}Si_6$ film and 70 ± 30 nm for the pure Ti film.

The quality of the thin films is a factor of corrosion resistant. Therefore, the surface morphology of thin films was examined by SEM and AFM. Examples are presented in Fig. 2. Basically, the surfaces of the as-sputtered fully amorphous Ti–Zr–Si thin films are quite smooth and featureless without grain boundaries, with the roughness Ra reading around 1 nm, much lower than the average roughness about 2 nm for the partially amorphous $Ti_{75}Zr_{19}Si_6$ TFMGC film or about 3–5 nm for the crystalline pure Ti. The morphology and the roughness of thin films with an amorphous structure are typically smoother than those of the crystalline counterparts. The smooth and uniform film quality is considered to be benefit for corrosion resistance.

For biomedical applications, both the biocompatibility and mechanical properties are of concern. Nanoindentation is perfect to extract the mechanical and wear behavior. Table 1 lists the measured data on the as-sputtered Ti–Zr–Si thin films. The modulus datum E on these four TFMGs or TFMGCs, $Ti_{47}Zr_{41}Si_{12}$, $Ti_{58}Zr_{33}Si_9$, $Ti_{66}Zr_{25}Si_9$ and $Ti_{75}Zr_{19}Si_6$, is 109, 115, 116 and 110 GPa, respectively, all lower than the 135 GPa for crystalline pure Ti. The amorphous random atomic structure with free volume does result in lower moduli. The nano-scaled hardness reading H of the $Ti_{47}Zr_{41}Si_{12}$, $Ti_{58}Zr_{33}Si_9$, $Ti_{66}Zr_{25}Si_9$ and $Ti_{75}Zr_{19}Si_6$ films is 5.2, 5.3, 6.2 and 4.8 GPa, respectively, all much higher than the ~2.0 GPa for crystalline pure Ti. The absence of dislocations, staking faults or twins would substantially increase the material hardness (and strength). In general, materials with higher hardness would be generally inherent with higher wear resistance Wr, as expressed by $Wr = H/E$ [23–25]. As the result, the current Ti-based TFMGs possess lower modulus but higher hardness/wear/strength natures, more promising than pure Ti in terms of their mechanical performance. Recently, Abdi et al. [26] have also reported that the high Ti-content $Ti_{75}Zr_{10}Si_{15}$ ribbons or rods with nanocrystalline β-Ti possess very high hardness, implying high wear resistance. In comparison, the current sputtered $T_{75}Zr_{19}Si_6$ thin film with nanrocrystalline α-Ti possesses lower hardness (4.8 GPa) than the much higher hardness (8.98–12.2 GPa) for the rapidly quenched $Ti_{75}Zr_{10}Si_{15}$ amorphous ribbons and rods with nanrocrystalline β-Ti, presumably due to the lower hardness of α-Ti than β-Ti [27]. It is interesting to systematically study the wear performance for all these Ti–Zr–Si coating films. Detailed characterization in terms of wear and adhesion testing of the sputtered films will be presented elsewhere.

3.2. Biocompatibility response

Before the starting potentiodynamic polarization test, the open circuit potential (OCP) measurements for all the five materials in SBF at 37 °C show the initial low potentials, being very slightly increasing to nobler potential with increasing immersion time up to 11,000 s. This suggests that, firstly, all of the Ti-based TFMGs and pure Ti were spontaneously oxidized in SBF, and, secondly, the passive oxide films would gradually become thickened [28]. There is no markedly fluctuation in the curves of $Ti_{47}Zr_{41}Si_{12}$, $Ti_{58}Zr_{33}Si_9$, $Ti_{66}Zr_{25}Si_9$, $Ti_{75}Zr_{19}Si_6$ and pure Ti over the time period of examination, implying the stable protective oxide films, as revealed later by the XPS results.

The potentiodynamic polarization Tafel curves in Fig. 3 and the data in Table 1 indicate that the E_{corr} would increase with increasing Ti content, from −0.53 to −0.32 V, approaching to the −0.32 V for the pure Ti. The normal human cell membrane environment has a potential of +0.08 V, thus all the four TFMGs and pure Ti cannot prevent from oxidation; or the formation of oxide layers is inevitable. For the Ti based metals, forming the TiO_2 oxide layer is not a negative issue. It is the severe pitting corrosion that would matter. In Fig. 3, there is no sign of pitting for all of four films, or the E_{pit} would be all over +2.0 V (Table 1). The stable potential regime with stable oxide layers without pitting, ΔE (=$E_{pit} - E_{corr}$), for these four Ti-based materials are all over 2.0 V (Table 1). The bio-corrosion potentials of the current Ti–Zr–Si TFMGs all pass the in vitro testing.

As compared in Table 1, the corrosion current densities, I_{corr}, of $Ti_{47}Zr_{41}Si_{12}$, $Ti_{58}Zr_{33}Si_9$, $Ti_{66}Zr_{25}Si_9$, $Ti_{75}Zr_{19}Si_6$ and pure Ti are 16.4×10^{-8}, 8.6×10^{-8}, 8.1×10^{-8}, 29.6×10^{-8} and 31.9×10^{-8} A/cm^2, respectively. The I_{corr} readings of the TFMG films

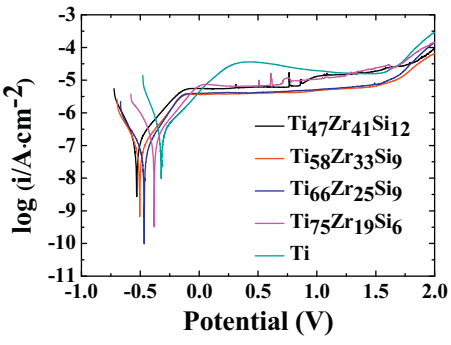

Fig. 3. Comparison of the Tafel potentiodynamic polarization curves of the pure Ti and the Ti–Zr–Si TFMGs in SBF at 37°C.

Table 1
The Young's modulus and hardness (extracted from nano-indentation), electrochemical parameters, corrosion current density (I_{corr}), corrosion potential (E_{corr}) and corrosion resistance (R_p), obtained from the potentiodynamic polarization curves of pure Ti and the Ti–Zr–Si as-deposited thin films at 37 °C in SBF. The electrochemical parameters are presented by the mean values with the standard errors and all the specimens are tested at least three times for the reproducibility. For the pitting voltage, we do not see any pitting up to the level of 2 V, thus E_{pit} should all be greater than 2 V.

	$Ti_{47}Zr_{41}Si_{12}$	$Ti_{58}Zr_{33}Si_9$	$Ti_{66}Zr_{25}Si_9$	$Ti_{75}Zr_{19}Si_6$	Ti
Young's modulus E (GPa)	109 ± 5	115 ± 4	116 ± 5	110 ± 5	135 ± 6
Hardness H (GPa)	5.2 ± 0.2	5.3 ± 0.3	6.2 ± 0.2	4.8 ± 0.1	2.0 ± 0.1
E_{corr} (V)	−0.53 ± 0.01	−0.50 ± 0.01	−0.46 ± 0.02	−0.37 ± 0.02	−0.32 ± 0.01
E_{pit} (V)	>2.0	>2.0	>2.0	>2/0	>2.0
ΔE (V)	>2.0	>2.0	>2.0	>2.0	>2.0
I_{corr} (10^{-8} A/cm^2)	16.4 ± 2.5	8.6 ± 0.3	8.1 ± 1.8	29.6 ± 1.6	31.9 ± 0.8
I_{pass} (10^{-8} A/cm^2)	2070 ± 86	420 ± 18	550 ± 40	1690 ± 14	2060 ± 77
R_p (10^5 Ω cm^2)	3.80 ± 2.96	5.56 ± 1.73	5.70 ± 1.94	3.78 ± 1.33	3.73 ± 2.45

were all lower than crystalline pure Ti, particularly for $Ti_{66}Zr_{25}Si_9$ (only 1/4 of the corrosion reaction current), indicating that the amorphous $Ti_{66}Zr_{25}Si_{19}$ film would form denser and more protective films in SBF. Meanwhile, the passive current densities, I_{pass}, in Table 1 of the TFMGs are also basically lower than that of pure Ti, suggesting the more stable and more protective oxide layers in the Ti–Zr–Si films. This is supported by the XPS results below. Overall, the current density I_{corr} and I_{pass} measurements ensure that the four Ti–Zr–Si TFMGs/TFMGCs can all easily pass the in vitro testing.

With the denser, more stable and more protective oxide layers on the Ti–Zr–Si TFMGs, the electrochemical AC impedance of the TFMGs should be higher than that of pure Ti. This can be justified by the so-called Nyquist plot to illustrate the electrochemical impedance spectra (EIS) for evaluating the polarization resistance (R_p). Fig. 4 shows the fitted data via the Nyquist plot for the Ti–Zr–Si TFMGs and pure Ti. The larger diameter of the semi-circle means the better bio-corrosion resistance. It obviously shows that the fully amorphous $Ti_{66}Zr_{25}Si_9$ TFMG possesses the best corrosion resistance. The R_p reading is 5.70×10^5 Ω for the fully amorphous $Ti_{66}Zr_{25}Si_9$, 5.56×10^5 Ω for $Ti_{58}Zr_{33}Si_9$, 3.80×10^5 Ω for $Ti_{47}Zr_{41}Si_{12}$, 3.78×10^5 Ω for the partially crystallized $Ti_{75}Zr_{19}Si_6$, all greater than the 3.73×10^5 Ω for crystalline pure Ti, as also compared in Table 1. Even with some nano-particles in the $Ti_{75}Zr_{19}Si_6$ composite film, its R_p value of 3.78×10^5 Ω for is still slightly higher than the 3.73×10^5 Ω for pure Ti. The R_p impedance value of $Ti_{66}Zr_{25}Si_9$ is 1.5 times of that of pure Ti, suggesting that the amorphous $Ti_{66}Zr_{25}Si_9$ thin film is apparently more promising than pure Ti in terms of bio-corrosion resistance in SBF.

The above results consistently reveal that, among the three fully amorphous films, the fully amorphous $Ti_{66}Zr_{25}Si_9$ film possesses the best performance, with the highest hardness, highest E_{corr}, lowest I_{corr} and I_{pass}, as well as the highest R_p. Since these three are all fully amorphous films with similar atomic structure and surface roughness, it is postulated that the composition would result in this bio-corrosion difference. With increasing Ti content in the three fully amorphous films, the TiO_2 oxide layer on the surface would obviously be thicker in the $Ti_{66}Zr_{25}Si_9$ film (as supported by the XPS results presented below). The thicker oxide layer can provide stronger protection, resulting in higher E_{corr} and R_p and lower I_{corr} and I_{pass}, all characteristic of higher corrosion resistance.

But with further increase in Ti content from 66 at% to 75 at% or even to 100 at%, the nanocrystalline HCP α-Ti phase would appear. The interfaces between the α-Ti nanocrystalline particles and the amorphous matrix in the partially crystallized $Ti_{75}Zr_{19}Si_6$ film would induce preferential corrosion, lowering the corrosion resistance, as evident from the rapid increase of I_{corr} and I_{pass} and the sudden decrease of R_p in Table 1. With further increase of Ti to the

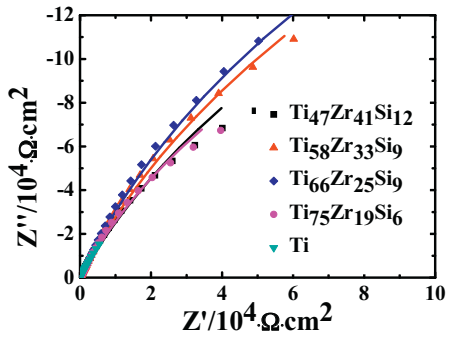

Fig. 4. Comparison of the EIS AC impedance testing for pure Ti and the Ti–Zr–Si TFMGs in SBF at 37°C.

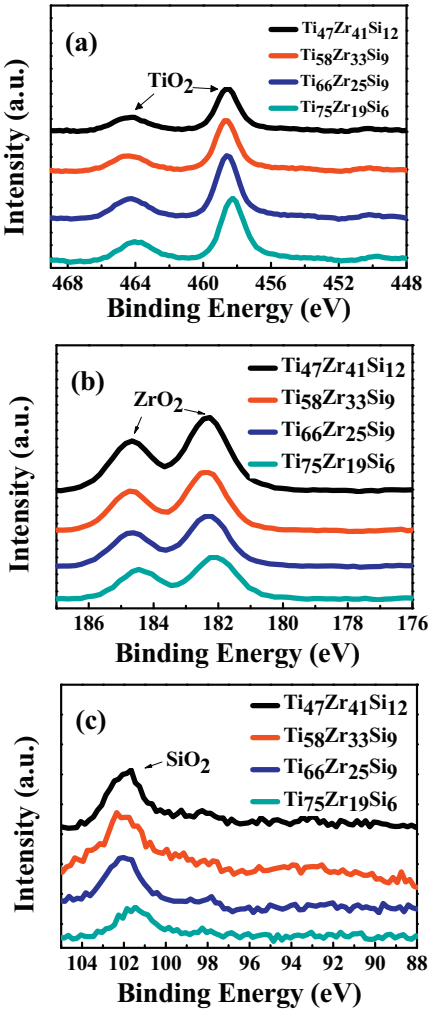

Fig. 5. The XPS spectra of the Ti–Zr–Si TFMGs surfaces for the peaks of (a) Ti2p, (b) Zr3d, and (c) Si2p.

100 at% pure Ti, the film contain nanocrystalline HCP α-Ti grains, with a grain size about 70 nm. The numerous grain boundaries in this pure Ti film, also coupled with higher surface roughness, would be inherent with even higher readings of I_{corr} and I_{pass} and an even lower reading of R_p as listed in Table 1. The overall bio-corrosion resistance trend of the current five sputtered films reveals an increasing resistance from the fully amorphous $Ti_{47}Zr_{41}Si_{12}$, $Ti_{58}Zr_{33}Si_9$ to $Ti_{66}Zr_{25}Si_9$ films, and then decreasing resistance in $Ti_{75}Zr_{19}Si_6$ and further decrease in pure Ti. The optimum is located at the $Ti_{66}Zr_{25}Si_9$ fully amorphous film.

It is always of interest to explore what the corrosion product layers would form in the current Ti–Zr–Si TFMGs in SBF. Fig. 5 presents the XPS spectra, clearly showing the two dominant TiO_2 and ZrO_2 oxide layers, along with minor SiO_2, on the film surfaces (to the inner depth about ~2 nm) after immersion in SBF for seven days. Note that the Ti-2p mixed peaks represent TiO_2 (with Ti-$2p_{3/2}$ at 458.1–458.8 eV and Ti-$2p_{1/2}$ at 464.0–464.5 eV). The Zr-3d peak consists of two peaks both originated from ZrO_2 (with Zr-$3d_{5/2}$ at 182.0–182.3 eV and Zr-$3d_{3/2}$ at 184.4–185.0 eV). And the Si-2p peak located at 101.4–102.3 eV corresponds to SiO_2. From Fig. 5(a), it can be seen that with increasing Ti content, the TiO_2 layer becomes thicker and denser, showing a higher Ti-2p peak. Our results are similar to the report by Kawashima et al. [29]. Their XPS results revealed that the Zr-based metallic glasses with higher Zr contents would form a higher concentration of Zr oxides in improving the corrosion resistance. For pure Ti film, there is only TiO_2 layer, but the four Ti–Zr–Si TFMGs would form TiO_2, ZrO_2 and SiO_2 compound oxide layers, upgrading the stability and protection nature in SBF. This might be another superior aspect of the Ti–Zr–Si TFMGs for bio-response. Note that the partially crystallized $Ti_{75}Zr_{19}Si_6$ film still possess the higher TiO_2 peak in Fig. 5(a), but the preferential corrosion along the interfaces between the α-Ti nano-crystalline particles and the amorphous matrix would impose a negative effect. Partial crystallization of the TFMGs will downgrade the bio-corrosion resistance.

4. Conclusions

In summary, the bio-friendly Ti–Zr–Si TFMGs are for the first time systematically examined by the bio-electrochemical testing. The following conclusions can be drawn.

(1) The sputtered Ti–Zr–Si TFMGs possess flatter, more uniform and higher quality surface morphology than the crystalline counterparts, with much lower roughness in the level of ~1 nm, highly favorable for subsequent biocompatibility and bio-corrosion testing.
(2) The Ti–Zr–Si TFMGs possess lower modulus but higher hardness (or strength or wear resistance) than pure Ti, more favorable in matching the modulus and strength of human bone.
(3) Based on the XPS results, the surfaces of the Ti–Zr–Si TFMGs appear to contain denser TiO_2, ZrO_2 and SiO_2 compound oxide layers. With increasing Ti content in the Ti–Zr–Si TFMGs, the protective TiO_2 layer seems to be thicker and denser. The compound protective layers in TFMGs would provide higher protection as compared with the TiO_2 in pure Ti film.
(4) All of the critical parameters, such as E_{corr}, E_{corr}, ΔE, I_{corr}, I_{pass} and R_p, extracted from the potentiodynamic polarization Tafel curves, the time-dependent open circuit potential (OCP) measurements, and EIS polarization resistance testing reveal that the Ti–Zr–Si TFMGs are either compatible or even superior to pure Ti, especially for the higher-Ti-content $Ti_{66}Zr_{25}Si_9$ fully amorphous film.
(5) The preferential corrosion along the interfaces between the α-Ti nano-crystalline particles and the amorphous matrix in the partially crystallized $Ti_{75}Zr_{19}Si_6$ film, or along the numerous grain boundaries in the nanocrystalline pure Ti film, would impose negative consequence. Partial crystallization of the TFMGs will downgrade the bio-corrosion resistance.
(6) The overall bio-corrosion resistance trend of the current five sputtered films reveals an increasing resistance from the fully amorphous $Ti_{47}Zr_{41}Si_{12}$, $Ti_{58}Zr_{33}Si_9$ to $Ti_{66}Zr_{25}Si_9$ films, and then decreasing resistance in $Ti_{75}Zr_{19}Si_6$ and further decrease in pure Ti. The optimum is located at the $Ti_{66}Zr_{25}Si_9$ fully amorphous film. Because Ti is a corrosion-resistant and easily oxidized element, the corrosion resistance of amorphous Ti–Zr–Si thin films in SBF can be related to the increasing Ti content. Nevertheless, when the Ti content is too high (~75 at%), the corrosion resistance would be reduced due to high electrochemical activity sites at the interfaces between the nanocrystalline phases and amorphous matrix. Therefore, increasing the Ti content but maintaining the amorphous structure becomes the key factor for improving the bio-corrosion behavior of the Ti–Zr–Si thin films.
(7) Judging from all of the above bio-corrosion and mechanical aspects, the developed Ti–Zr–Si amorphous films are considered to be highly promising coating biomaterials.

Acknowledgement

The authors gratefully acknowledge the sponsorship from National Science Council of Taiwan, ROC, under the project No. NSC101-2120-M-110-007.

References

[1] M. Long, H.J. Rack, Titanium alloys in total joint replacement, Biomaterials 19 (1998) 1621–1639.
[2] R. Banerjee, S. Nag, J. Stechschulte, H.L. Fraser, Strengthening mechanisms in Ti–Nb–Zr–Ta and Ti–Mo–Zr–Fe orthopedic alloys, Biomaterials 25 (2004) 3413–3419.
[3] L. Hao, J. Lawrence, L. Li, Manipulation of the osteoblast response to a Ti–6Al–4V titanium alloy using a high power diode laser, Appl. Surf. Sci. 247 (2005) 602–606.
[4] M.P. Staigera, A.M. Pietaka, J. Huadmaia, G. Diasb, Magnesium and its alloys as orthopedic biomaterials: a review, Biomaterials 27 (2006) 1728–1734.
[5] Y. Wu, A.H. Wanga, Z. Zhanga, R.R. Zhenga, H.B. Xiab, Y.N. Wang, Laser alloying of Ti–Si compound coating on Ti–6Al–4V alloy for the improvement of bioactivity, Appl. Surf. Sci. 305 (2014) 16–23.
[6] Y.F. Zheng, D. Liu, X.L. Liu, L. Li, Enhanced corrosion resistance of Zr coating on biomedical TiNi alloy prepared by plasma immersion ion implantation and deposition, Appl. Surf. Sci. 255 (2008) 512–514.
[7] T. Zhang, A. Inoue, T. Masumoto, Amorphous (Ti, Zr, Hf)–Ni–Cu ternary alloys with a wide supercooled liquid region, Mater. Sci. Eng. A 181 (1994) 1423–1426.
[8] A. Inoue, N. Nishiyama, K. Amiya, T. Zhang, T. Masumoto, Ti-based amorphous alloys with a wide supercooled liquid region, Mater. Lett. 19 (1994) 131–135.
[9] K. Amiya, N. Nishiyama, A. Inoue, T. Masumoto, Mechanical strength and thermal stability of Ti-based amorphous alloys with large glass-forming ability, Mater. Sci. Eng. A 179–180 (1994) 692–696.
[10] T. Zhang, A. Inoue, Thermal and mechanical properties of Ti–Ni–Cu–Sn amorphous alloys with a wide supercooled liquid region before Crystallization, Mater. Trans. JIM 39 (1998) 1001–1006.
[11] T. Zhang, A. Inoue, Ti-based amorphous alloys with a large supercooled liquid region, Mater. Sci. Eng. A 304–306 (2001) 771–774.
[12] J.M. Park, Y.C. Kim, W.T. Kim, D.H. Kim, Ti-based bulk metallic glasses with high specific strength, Mater. Trans. 45 (2004) 595–598.
[13] F.X. Qin, M. Yoshimura, X.M. Wang, S.L. Zhu, A. Kawashima, K. Asami, A. Inoue, Fabrication and corrosion property of novel Ti-based bulk glassy alloys without Ni, Mater. Trans. 48 (2007) 515–518.
[14] J.J. Oak, A. Inoue, Attempt to develop Ti-based amorphous alloys for biomaterials, Mater. Sci. Eng. A 449-451 (2007) 220–224.
[15] J.P. Chu, J.S.C. Jang, J.C. Huang, H.S. Chou, Y. Yang, J.C. Ye, Y.C. Wang, J.W. Lee, F.X. Liu, P.K. Liaw, Y.C. Chen, C.M. Lee, C.L. Li, C. Rullyani, Thin film metallic glasses: unique properties and potential applications, Thin Solid Films 520 (2012) 5097–5122.
[16] Y.Y. Chu, Y.S. Lin, C.M. Chang, J.-K. Liu, C.H. Chen, J.C. Huang, Promising antimicrobial capability of thin film metallic glasses, Mater. Sci. Eng. C C6 (2014) 221–225.

[17] G. Xie, F. Qin, S. Zhu, D.V. Louzguine-Lugzin, Corrosion behaviour of porous Ni-free Ti-based bulk metallic glass produced by spark plasma sintering in Hanks' solution, Intermetallics 44 (2014) 55–59.
[18] J. Jayaraj, J.M. Parka, P.F. Gostin, E. Fleury, A. Gebert, L. Schultz, Nano-porous surface states of Ti–Y–Al–Co phase separated metallic glass, Intermetallics 17 (2009) 1120–1123.
[19] J. Jayaraj, B.J. Park, D.H. Kim, W.T. Kim, E. Fleury, Nanometer-sized porous Ti-based metallic glass, Scr. Mater. 55 (2006) 1063–1066.
[20] S.L. Zhu, X.M. Wang, F.X. Qin, A. Inoue, A new Ti-based bulk glassy alloy with potential for biomedical application, Mater. Sci. Eng. A 459 (2007) 233–237.
[21] M. Calin, A. Gebert, A.C. Ghinea, P.F. Gostin, S. Abdi, C. Mickel, Designing biocompatible Ti-based metallic glasses for implant applications, Mater. Sci. Eng. C 33 (2013) 875–883.
[22] B.E. Warren, X-Ray Diffraction, Addison-Wesley Pub. Inc, London, 1969.
[23] K.H. Frosch, K.M. Stürmer, Metallic biomaterials in skeletal repair, Eur. J. Trauma 32 (2006) 149–159.
[24] J.A. Disegi, Titanium alloys for fracture fixation implants, Injury 31 (2000) D14–D17.
[25] S.F. Guo, L. Liu, N. Li, Y. Li, Fe-based bulk metallic glass matrix composite with large, Scr. Mater. 62 (2010) 329–332.
[26] S. Abdi, M.S. Khoshkhoo, O. Shuleshova, M. Bönisch, M. Calin, L. Schultz, J. Eckert, M.D. Baró, J. Sort, A. Gebert, Effect of Nb addition on microstructure evolution and nanomechanical properties of a glass-forming Ti–Zr–Si alloy, Intermetallics 46 (2014) 156–163.
[27] Y.L. Kao, G.C. Tu, C.A. Huang, T.T. Liu, A study on the hardness variation of α- and β-pure titanium with different grain size, Mater. Sci. Eng. A 398 (2005) 93–98.
[28] C. Lavos-Valereto, I. Costa, S. Wolynec, The electrochemical behavior of Ti-6Al-7Nb alloy with and without plasma-sprayed hydroxyapatite coating in Hank's solution, J. Biomed. Mater. Res. 63 (2002) 664–670.
[29] A. Kawashima, K. Ohmura, Y. Yokoyama, A. Inoue, The corrosion behaviour of Zr-based bulk metallic glasses in 0.5 M NaCl solution, Corros. Sci. 53 (2011) 78–2784.